

Generation of spatiotemporal acoustic vortices with arbitrarily oriented orbital angular momentum

Received: 28 June 2024

Accepted: 11 March 2025

Published online: 22 March 2025

Shuai Liu^{1,5}, Hao Ge^{1,5}✉, Xiang-Yuan Xu¹, Yuan Sun¹, Xiao-Ping Liu², Ming-Hui Lu^{1,3,4}✉ & Yan-Feng Chen^{1,4}✉

Despite extensive exploration of acoustic vortices carrying orbital angular momentum (OAM), the generation of acoustic vortices with OAM orientations beyond the conventional longitudinal direction remains largely unexplored. Spatiotemporal (ST) vortices, featuring spiral phase twisting in the ST domain and carrying transverse OAM, have recently attracted considerable interest in optics and acoustics. Here, we report the generation of three-dimensional (3D) ST acoustic vortices with arbitrarily oriented OAM, thereby opening up a new dimension in acoustic OAM control. By utilizing a two-dimensional (2D) acoustic phased array, we introduce two approaches to manipulate the orientation of OAM: through the direct rotation of vortices in 3D space and the intersection of vortices carrying distinct types of OAM. These methods enable unprecedented control over the orientation of acoustic OAM, providing a new degree of freedom in the manipulation of acoustic waves. The arbitrarily oriented OAM may enable more complex particle manipulation techniques. Our work establishes a foundation for future explorations into the complex dynamics of novel structured acoustic fields in the ST domain.

Vortices are ubiquitous phenomena across various domains of physics and have been extensively studied and generated in diverse wave fields, including electromagnetic waves^{1–5}, acoustic waves^{6–12}, electron waves¹³, and neutron waves¹⁴. Optical and acoustic vortices are characterized by a doughnut-shaped intensity distribution and a spiral phase distribution, and they can carry longitudinal orbital angular momentum (OAM) aligned with their propagation direction. The longitudinal OAM carried by vortex beams provides a new degree of freedom and has been widely utilized in applications such as information transmission^{15–17}, super-resolution imaging¹⁸, quantum key distribution¹⁹, and particle manipulation^{20–23}.

Recently, there has been a growing interest in spatiotemporal (ST) vortices where the wave packets are structured in both space and time^{24–34}. Differing from conventional monochromatic vortices with a

spiral phase in the spatial domain, these vortices are polychromatic wave packets and exhibit a spiral phase in the ST domain. The energy circulation in the ST domain results in a transverse OAM perpendicular to the propagation direction. This transverse OAM provides a new degree of freedom which is expected to extend the functionalities of vortices, and leads to the discovery of novel physical phenomena, such as spin-orbit interaction between transverse spin and orbital angular momentum²⁸, transverse shifts and time delays of vortices at interfaces³⁵ and nonlinear optical harmonic generation with transverse OAM^{36–38}. Generating such transverse OAM requires simultaneously spatial and temporal modulations of wave packets. In optics, ST vortices were generated experimentally using sophisticated optical systems containing components like spatial light modulators and lenses³⁹. ST vortices can also be generated by designed structures such as

¹National Laboratory of Solid State Microstructures & Department of Materials Science and Engineering, Nanjing University, Nanjing, Jiangsu, China. ²School of Physical Science and Technology, ShanghaiTech University, Shanghai, China. ³Jiangsu Key Laboratory of Artificial Functional Materials, Nanjing, Jiangsu, China. ⁴Collaborative Innovation Center of Advanced Microstructures, Nanjing University, Nanjing, China. ⁵These authors contributed equally: Shuai Liu, Hao Ge. ✉ e-mail: haoge@nju.edu.cn; luminghui@nju.edu.cn; yfchen@nju.edu.cn

photonic crystal slabs and resonant diffractive gratings. The transmission function of these structures exhibits nodal lines in the wavevector-frequency space^{40–44}. Moreover, arbitrarily oriented optical vortices could be constructed^{40,45–47}, promising more controllable degree of freedoms and advanced applications.

Wave fields with OAM have also been widely investigated in the area of acoustics. Acoustic vortices can be generated by using a planar array of transducers^{7,48} or passive metasurface structures¹⁰. Several acoustic OAM-based applications were proposed, such as acoustic trapping⁴⁹, rotation⁵⁰, levitation⁵¹, and sound asymmetric transmission⁵². Acoustic communication by multiplexing OAM was also experimentally demonstrated, enabling high-speed data transmission for underwater applications¹⁶. Very recently, ST vortices have been explored in acoustics, bringing novel functionalities to acoustic OAM-based applications. The ST acoustic vortices are generated via a one-dimensional (1D) acoustic phased array⁵³ or a periodic meta-grating⁵⁴. These ST vortices propagate within the acoustic waveguide, which can be treated as a two-dimensional (2D) spatial geometry.

In this work, we advance our understanding of acoustic vortices by synthesizing three-dimensional (3D) ST acoustic vortices with OAM oriented in arbitrary directions, aiming for more comprehensive control over acoustic OAM. Compared to the 2D case, adding an additional dimension allows for the realization of more complex ST acoustic vortices. Unlike the methods used in optics, we decompose the ST vortices into a series of plane wave modes and generate them using an acoustic phased array. The 3D profile of ST acoustic vortices can be measured directly and precisely. We initially utilize a 2D acoustic phased array to generate 3D ST vortices carrying longitudinal and transverse OAM, respectively. To generate acoustic OAM with arbitrary orientations, we employ two distinct approaches. The first approach involves the direct rotation of wave packets carrying longitudinal or transverse OAM in 3D space, as depicted in Fig. 1a. The orientation of OAM will change accordingly. The second approach is achieved through the intersection of vortices carrying longitudinal and transverse OAM, as shown in Fig. 1b. The longitudinal and transverse OAM components can be modified, thereby altering the orientation of the OAM. The tilted OAM may be employed for more sophisticated particle manipulation through the transfer of acoustic OAM to particles. Our work establishes a platform for investigating 3D ST acoustic vortices and may open new avenues for exploring novel structured acoustic fields in the ST domain.

Results

Generation of three-dimensional (3D) spatiotemporal (ST) vortices with longitudinal and transverse orbital angular momentum (OAM)

Assuming that all wave packets propagate along the z -axis, we initially construct 3D ST acoustic wave packets carrying longitudinal and transverse OAM, respectively. The procedure is as follows: First, the analytical expression of the ST acoustic wave packet is derived, and a Fourier transform is applied to obtain its spatial frequency spectrum. From this spectrum, the intrinsic OAM of the ST acoustic wave packet is theoretically calculated. Next, the spatial frequency spectrum is sampled to extract a series of plane wave modes with specific frequencies and propagation directions. Experimentally, these plane wave modes are generated using an acoustic phased array. Finally, the superposition of these plane waves constructs the target ST acoustic wave packet.

To generate a 3D ST wave packet possessing longitudinal OAM along the z -axis, a spiral phase factor, $[x + i \cdot \text{sgn}(ly)]^{|l|}$, is introduced into the $x - y$ plane of a 3D Gaussian wave packet. Such a spiral phase will give rise to a phase singularity line along the z -axis, and l describes the number of times the phase wraps around the singularity line. Consequently, the amplitude at the center of the $x - y$ plane must be zero, which manifests as a tunnel along the z -axis on the 3D iso-intensity profile of the wave packet. The presence of such a tunnel results in the iso-intensity surface taking on a toroidal geometry. The acoustic

pressure field of this ST wave packet can be expressed as follows:

$$p(x, y, z, t) \propto [x + i \cdot \text{sgn}(ly)]^{|l|} e^{-\frac{x^2 + y^2 + \zeta^2}{w^2}} e^{ik_0 \zeta} \quad (1)$$

where k_0 is the central wavevector, $\zeta = z - ct$ is the pulse-accompanying coordinate, and c is the speed of acoustic wave. The widths of the wave packet along x , y , and z axes are identical and are defined by the parameter w . Similarly, we can add the phase factor $[\zeta + i \cdot \text{sgn}(lx)]^{|l|}$ into the $z - x$ plane (or the $t - x$ plane) of a 3D Gaussian wave packet, and the acoustic pressure field of the ST wave packet can be expressed as follows:

$$p(x, y, z, t) \propto [\zeta + i \cdot \text{sgn}(lx)]^{|l|} e^{-\frac{x^2 + y^2 + \zeta^2}{w^2}} e^{ik_0 \zeta} \quad (2)$$

The ST wave packet is a polychromatic beam that can be constructed through the superposition of a series of plane wave modes $P(\mathbf{k})e^{i\mathbf{k} \cdot \mathbf{r} - i\omega(\mathbf{k})t}$, where $P(\mathbf{k})$ is the complex plane-wave amplitudes. $P(\mathbf{k})$ can be obtained through a Fourier transform, and represents the spatial frequency spectrum of the acoustic pressure field. The normalized integral values of OAM can be calculated using $P(\mathbf{k})$ as⁵⁵:

$$\mathbf{L} = \frac{\int \omega^{-1} P^* (-i\mathbf{k} \times \nabla_{\mathbf{k}}) P d^3 \mathbf{k}}{\int \omega^{-1} |P|^2 d^3 \mathbf{k}}. \quad (3)$$

It is worth noting that the OAM consists of both intrinsic and extrinsic components. The extrinsic component originates from the transverse shift of the pulse probability centroid \mathbf{R} , which is defined as⁵⁵:

$$\mathbf{R} = \frac{\int \omega^{-1} P^* e^{i\omega t} (i\nabla_{\mathbf{k}}) P e^{-i\omega t} d^3 \mathbf{k}}{\int \omega^{-1} |P|^2 d^3 \mathbf{k}}. \quad (4)$$

The extrinsic component satisfies $\mathbf{L}^{\text{ext}} = \mathbf{R}k_0$, and we can obtain the intrinsic component as:

$$\mathbf{L}^{\text{int}} = \mathbf{L} - \mathbf{L}^{\text{ext}}. \quad (5)$$

The calculated \mathbf{L}^{int} of the two wave packets defined by Eqs. (1) and (2) are $(0, 0, l)$ and $(0, l, 0)$, which confirms that these two wave packets carry longitudinal and transverse OAM, respectively.

We then sample the spatial frequency spectrum to extract a series of plane wave modes, each defined by specific frequencies and propagation directions. In the spatial frequency domain, centered at $(0, 0, k_0)$, with $k_0 = 75.1 \text{ m}^{-1}$, we sample 14 values in each of the k_x , k_y , and k_z directions with an interval of $0.046k_0$, resulting in a total of 2744 modes. The corresponding frequency range is 2873 – 5607 Hz. These 2744 plane wave modes are then generated using a 2D acoustic phased array to construct the ST wave packet through their superposition. The resulting wave packet will exhibit a spatial width of approximately 70 cm and a temporal duration of around 2 ms.

Our experimental setup is schematically shown in Fig. 1c–e. The experiment is conducted in an anechoic chamber to mitigate the impact of reflections on the measurements. The 121 speakers are arranged in an 11×11 2D square grid with a spacing of 5.5 cm between each row and column, forming a 2D acoustic phased array. Each speaker is controlled by an individual channel of a sound card, allowing independent adjustment of its amplitude and phase [see Methods for details]. By adjusting the phase of each speaker element in the array, the propagation direction of the acoustic wave can be controlled, enabling the generation of a plane wave mode with the desired direction. By simultaneously generating the selected 2744 plane wave modes, the ST wave packet can be constructed.

The 3D ST acoustic wave packet can be characterized either in the $x - y - z$ space by a time snapshot or the $x - y - t$ spatial-temporal

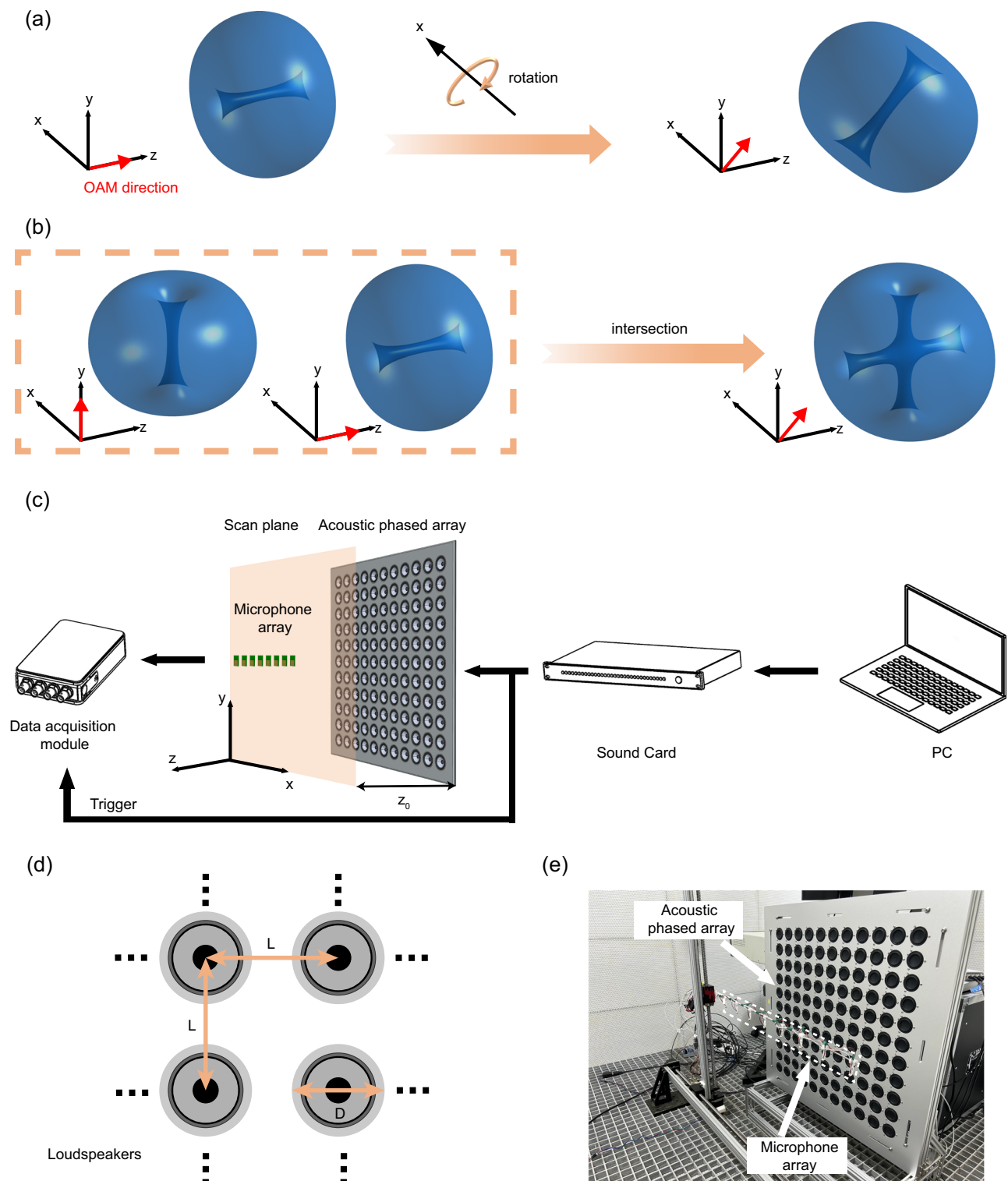


Fig. 1 | Synthesizing three-dimensional (3D) spatiotemporal (ST) acoustic vortices with orbital angular momentum (OAM) oriented in arbitrary directions. **a** Direct rotation of ST acoustic vortices in 3D space. A ST wave packet carrying longitudinal OAM is rotated around the x -axis, and the direction of OAM will change accordingly, which is indicated by the red arrow in the coordinate system. **b** Intersection of ST vortices carrying transverse and longitudinal OAM yields a ST wave packet carrying tilted OAM. **c** Schematic of experimental setup. Spatio-temporal vortices are generated by an acoustic phased array controlled by the sound cards. On the scanning plane at a distance of $z_0 = 20\text{ cm}$ from the acoustic

phased array, we measure the time-domain acoustic pressure signals using a microphone array. A trigger signal is generated simultaneously with the wave packet signal by the sound card and transmitted to the data acquisition module to initiate data collection, ensuring that each captured time-domain acoustic pressure signal is located within the same time interval. **d** The acoustic phased array consists of 121 loudspeakers with a diameter of $D = 4.3\text{ cm}$, arranged in a two-dimensional rectangular grid with a spacing of $L = 5.5\text{ cm}$. **e** Photograph of the experimental setup.

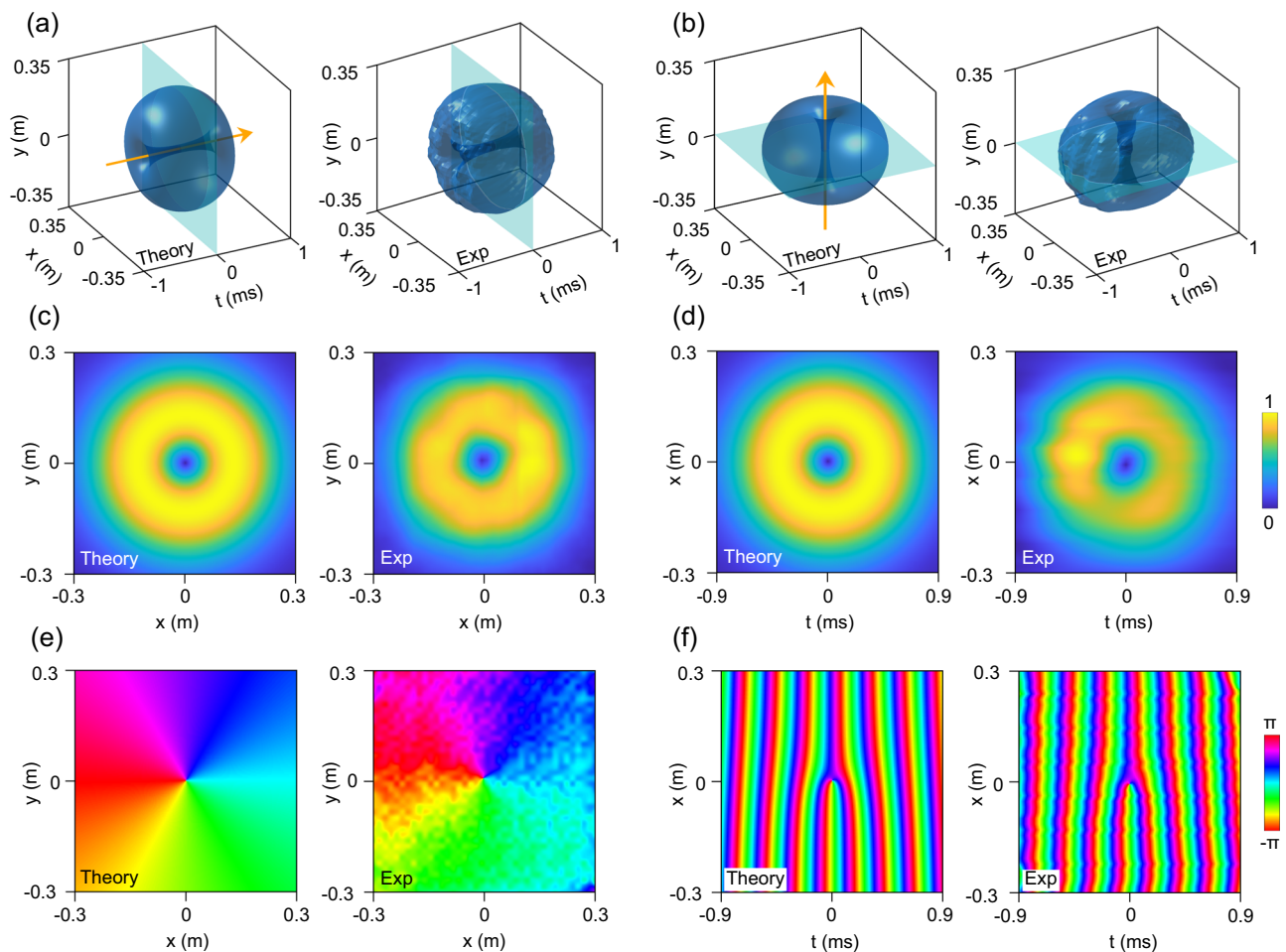


Fig. 2 | Three-dimensional (3D) spatiotemporal (ST) vortices with longitudinal and transverse orbital angular momentum (OAM). **a, b** The 3D iso-intensity profiles of the ST wave packets carrying longitudinal OAM and transverse OAM. The maximum intensity is set to 1, with isovalue at 0.0625, meaning that the iso-intensity profile includes all points with intensity greater than 0.0625. The orange arrows indicate the direction of OAM carried by the wave packet. **c, e** The amplitude

and phase distributions of the cross-section passing through the center of the wave packets carrying longitudinal OAM (the cyan plane in **(a)**), which show the screw phase dislocation. **d, f** The amplitude and phase distributions of the cross-section passing through the center of the wave packets carrying transverse OAM (the cyan plane in **(b)**), which show the edge phase dislocation.

domain at a fixed z position. Here, we adopt the latter characterization method, measuring the time-domain signals using microphones at each point within the $z=0$ plane (the orange region in Fig. 1c), as depicted in Fig. 1c, e. The measurement step size in the x - and y - directions is 1.5 cm. In the experiment, the central frequency of 4100 Hz corresponds to a wavelength of 8.4 cm. The scanning step size is approximately 0.18 times the corresponding wavelength, ensuring accurate characterization of the acoustic field. For each measurement, the phased array generates the ST wave packet, and a segment of the time-domain acoustic pressure signal is recorded using the microphone. We employ a separate pulse signal from the sound card to synchronously trigger each recording session. The measured signal corresponds to the real part of the acoustic pressure field. By applying the Hilbert transform to the time-domain signal, the imaginary part can be obtained, providing the full complex representation of the acoustic pressure field [see Supplementary Section 3 for details]. This approach enables direct determination of the amplitude and phase distribution of acoustic field.

The 3D iso-intensity profiles of the ST wave packets carrying longitudinal and transverse OAM, obtained through both theoretical calculations and experimental measurements, are shown in Fig. 2a and b, respectively. The t term for both vortices are set to 1. The time $t=0$ corresponds to the moment when the center position of the wave packet reaches $z=0$. The orange arrows in Fig. 2a, b indicate the

direction of the OAM carried by the corresponding wave packets. It can be observed that the experimental measurements are consistent with the theoretical predictions. Due to the spiral phase within the $x-y$ plane, there is a phase singularity line along the z -axis, resulting in a tunnel in the direction of the z -axis for the wave packet carrying longitudinal OAM, as shown in Fig. 2a. Similarly, for the wave packet carrying transverse OAM, it exhibits a helical phase in the $t-x$ plane and a singularity line along the y -axis, leading to a tunnel parallel to the y -axis, as depicted in Fig. 2b. We present theoretical calculations and experimental measurements of the amplitude and phase distributions of cross-sections passing through the centers of the two types of wave packets (the cyan planes in Fig. 2a, b). As shown in Fig. 2c, d, both cross-sections exhibit annular amplitude distributions, which arise from the presence of phase singularities at the centers of the cross-sections for both types of vortices, resulting in zero intensity. The phase distributions of the cross-sections of the two types of wave packets are provided in Fig. 2e and f, respectively. As illustrated in Fig. 2e, the wave packet carrying longitudinal OAM exhibits a phase screw dislocation in the $x-y$ plane. In contrast, the wave packet carrying transverse OAM exhibits a characteristic edge phase dislocation in the $t-x$ plane, as depicted in Fig. 2f. We demonstrate that 3D ST wave packets carrying longitudinal and transverse OAM can be generated in acoustics, laying the foundation for manipulating the direction of OAM. Next, we follow

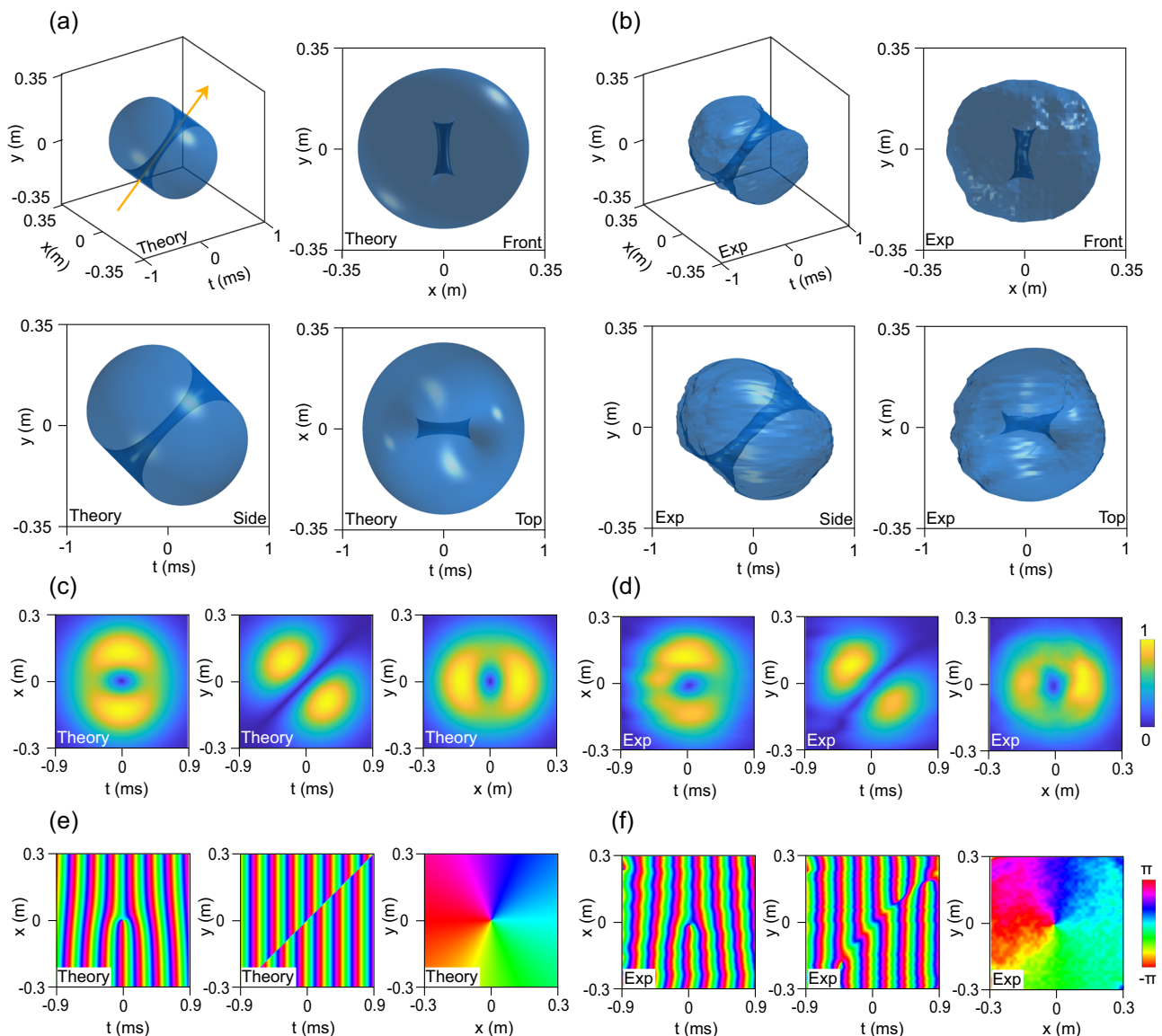


Fig. 3 | Direct rotation of spatiotemporal (ST) vortices in three-dimensional (3D) space. **a, b** The 3D iso-intensity profiles of the rotated ST wave packet, along with its front, side, and top views, obtained from theoretical calculations and experimental measurements. The maximum intensity is set to 1, with isovalue at 0.0625. The orange arrows indicate the direction of the orbital angular momentum

(OAM) carried by the wave packet, pointing towards $(0, \frac{\sqrt{2}}{2}, \frac{\sqrt{2}}{2})$. The amplitude and phase distributions of three cross-sections passing through the center of the wave packet, derived from both theoretical calculations and experimental measurements, are shown in (c), (d) and (e), (f), respectively.

the same procedure to generate rotated and intersected ST acoustic vortices.

Direct rotation of spatiotemporal (ST) vortices in three-dimensional (3D) space

While previous studies on acoustic OAM have primarily focused on longitudinal and transverse OAM, it is essential to recognize that acoustic OAM can exhibit arbitrary orientations. To alter the direction of the OAM, we can directly rotate the wave packet carrying transverse or longitudinal OAM in 3D space. Here, we take the example of rotating a wave packet carrying longitudinal OAM. Considering a 45-degree rotation around the x -axis of the acoustic pressure field described in Eq. (1) and setting $l = 1$, the rotated wave packet is expressed as:

$$p(x, y, z, t) \propto \left[x + i \left(\frac{\sqrt{2}}{2} y - \frac{\sqrt{2}}{2} z \right) \right] e^{-\frac{x^2 + y^2 + z^2}{w^2}} e^{ik_0 \zeta}. \quad (6)$$

The wave packet carrying longitudinal OAM is rotated without altering its propagation direction along the z -axis. The intrinsic OAM carried by the tilted wave packet can be calculated using Eqs. (3)–(5) as $(0, \frac{\sqrt{2}}{2}, \frac{\sqrt{2}}{2})$, indicating that the OAM direction also rotates 45 degrees around the x -axis. The 3D iso-intensity profiles, derived from both theoretical calculations and experimental measurements for the rotated wave packet, are illustrated in Fig. 3a, b, including perspective, front, side, and top views. The direction of the OAM after rotation is indicated by orange arrows in Fig. 3a. From the three views, it is evident that there is a tunnel tilted at a 45-degree angle upwards relative to the z -axis. This is because the singularity line is rotated from being aligned with the z -axis to a direction at a 45-degree angle to the z -axis. Figure 3c, d presents the amplitude distributions in the $t-x$, $t-y$, and $x-y$ cross-sections passing through the center of the wave packet, and Fig. 3e, f illustrate the corresponding phase distributions, based on both theoretical calculations and experimental measurements. Due to the rotation of the wave packet, the previously circular intensity

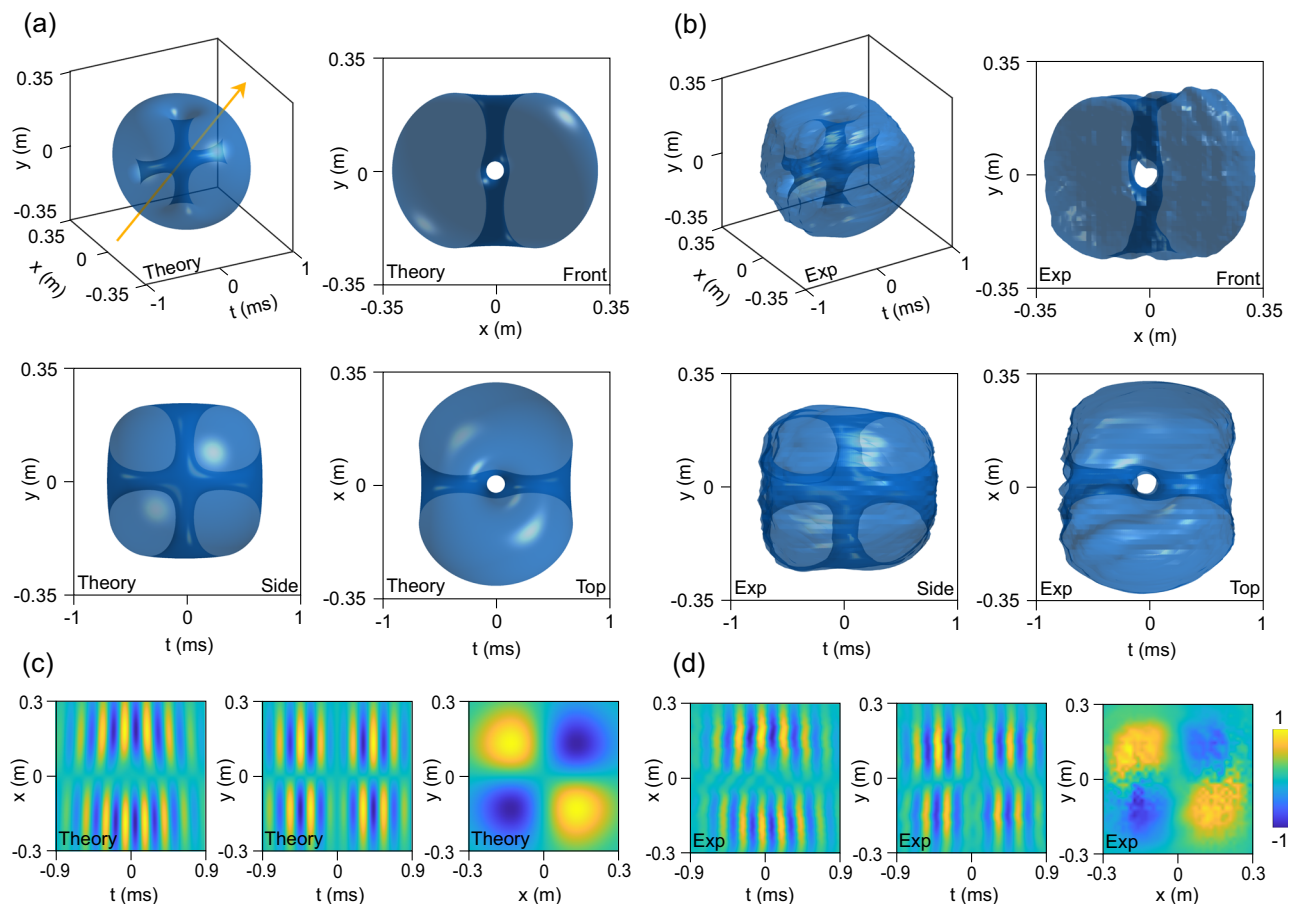


Fig. 4 | Intersection of vortices carrying longitudinal and transverse orbital angular momentum (OAM). **a, b** The three-dimensional iso-intensity profiles of the spatiotemporal wave packets combining two vortices carrying different types of OAM, obtained through theoretical calculations and experimental measurements. The maximum intensity is set to 1, with isovalue at 0.04. The orange arrows

indicate the direction of the OAM carried by the wave packet, pointing towards (0, 1, 1). **c, d** Theoretical calculation and experimental measurement results of the acoustic pressure field on the cross-sections passing through the center of the wave packet.

distribution on the $x-y$ plane is now rotated onto a plane with a normal vector of $(0, \frac{\sqrt{2}}{2}, \frac{\sqrt{2}}{2})$. The tilted annular intensity distribution obtained after rotation exhibits an elliptical intensity distribution on both the $t-x$ and $x-y$ cross-sections, while the diagonal line with zero intensity in the $t-y$ cross-section corresponds to the tilted tunnel passing through the center of the wave packet, as illustrated in Fig. 3c, d. The phase distribution in the $t-x$ cross-section exhibits an edge phase dislocation, corresponding to the transverse OAM component in the y -direction, while the phase distribution in the $x-y$ cross-section manifests a helical phase dislocation, corresponding to the longitudinal OAM component in the z -direction, as shown in Fig. 3e, f. Here, only an example of a wave packet rotating 45 degrees around the x -axis is shown. More generally, by controlling the direction and angle of rotation of the wave packet, the orientation of OAM can be precisely manipulated in the 3D space.

Intersection of vortices carrying longitudinal and transverse orbital angular momentum (OAM)

To vary the direction of the OAM, apart from rotating a wave packet carrying OAM in a particular direction, another method involves integrating vortices carrying different types of OAM within a single wave packet. For instance, the intersection of a vortex carrying longitudinal OAM and another carrying transverse OAM within a 3D Gaussian wave packet yields a wave packet carrying tilted OAM. The acoustic pressure distribution of the wave packet generated by the

intersection of two types of vortices is illustrated as follows:

$$p(x, y, z, t) \propto [x + i \cdot \text{sgn}(l_1)y]^{|l_1|} [\zeta + i \cdot \text{sgn}(l_2)x]^{|l_2|} e^{-\frac{x^2+y^2+\zeta^2}{w^2}} e^{ik_0\zeta} \quad (7)$$

where l_1 and l_2 denote the spiral phase in the $x-y$ domain and $z-x$ domain, respectively. The intrinsic OAM carried by the wave packet is calculated as $(0, l_2, l_1)$. By adjusting the values of l_1 and l_2 , we can change the orientation of the OAM in the $y-z$ plane. When we set l terms of both vortices to 1, the tilted OAM can be calculated using Eqs. (3)–(5), resulting in $(0, 1, 1)$. Figure 4a, b illustrates the 3D iso-intensity profiles of the wave packet represented by Eq. (7), obtained through both theoretical calculations and experimental measurements. The wave packet features two tunnels, with the t -axis direction tunnel arising from the helical phase in the $x-y$ plane and the y -axis direction channel originating from the helical phase in the $t-x$ plane. Figures 4c, d illustrates the acoustic pressure distribution in the $t-x$, $t-y$, and $x-y$ cross-sections passing through the center of the wave packet.

Furthermore, we demonstrate the intersection of three vortices carrying OAM in mutually perpendicular directions. By changing the l terms of the three vortices, the orientation of the OAM can be arbitrarily changed within the $x-y-z$ space. Figure 5a, b depicts the theoretical calculation results and experimental measurements of the iso-intensity profiles of the wave packet combining three vortices, each with a l term of 1. The calculated intrinsic OAM carried by the wave packet is $(1, 1, 1)$, as depicted by the orange arrow in Fig. 5a. The tunnel

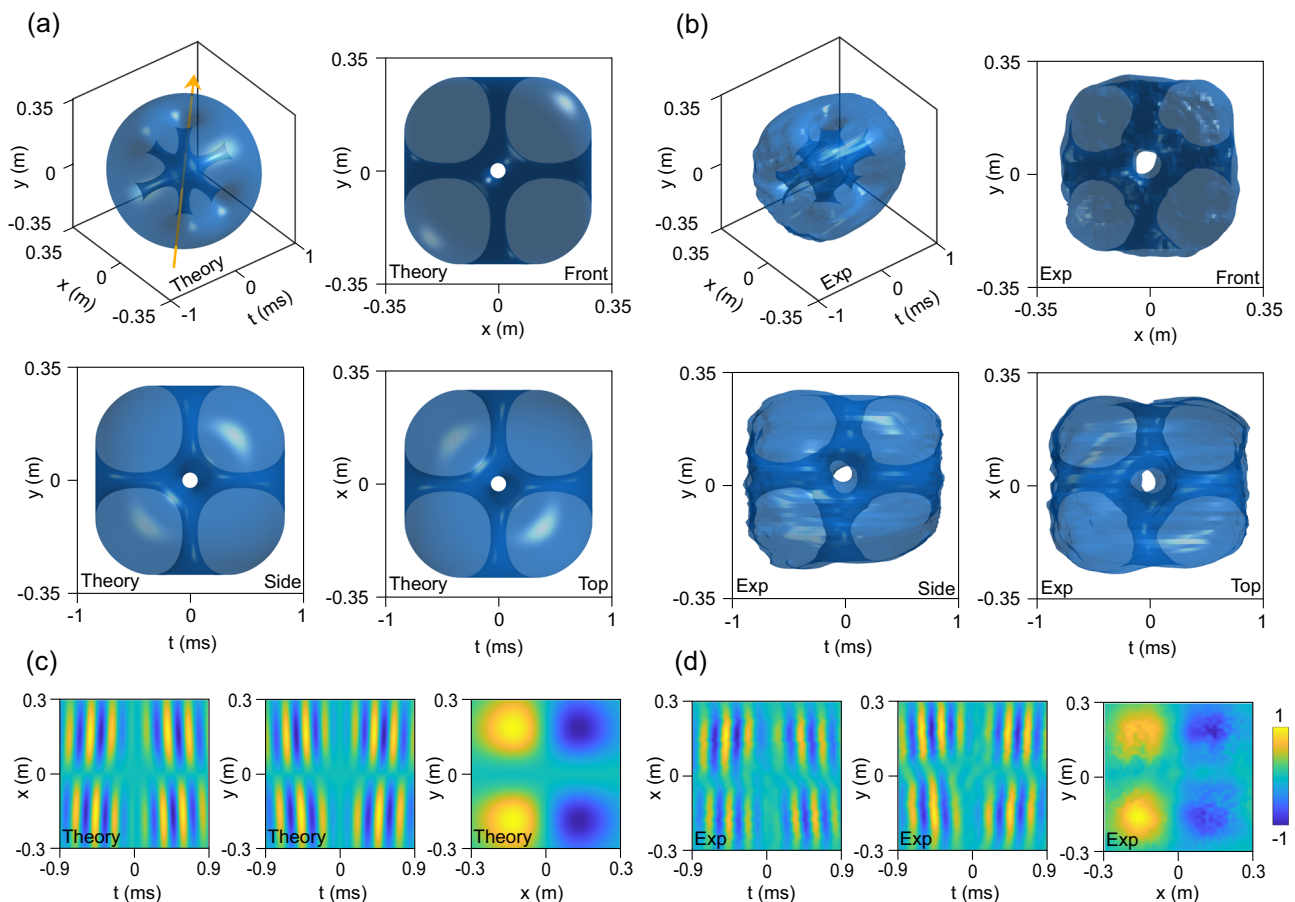


Fig. 5 | Intersection of three vortices carrying orbital angular momentum (OAM) in mutually perpendicular directions. **a, b** The three-dimensional isointensity profiles of the spatiotemporal wave packets combining three vortices, obtained through theoretical calculations and experimental measurements. The

maximum intensity is set to 1, with isovalue at 0.0841. The orange arrows indicate the direction of the OAM carried by the wave packet, pointing towards (1, 1, 1). **c, d** Theoretical calculation and experimental measurement results of the acoustic pressure field on the cross-sections passing through the center of the wave packet.

along the t -axis is attributed to the helical phase in the $x - y$ plane, whereas the tunnels along the x -axis and y -axis is caused by the helical phase in the $t - y$ plane and $t - x$ plane. This demonstrates that we can create complex zero-amplitude tunnel structures through the superposition of 3D ST vortices. The acoustic pressure fields of three cross-sections passing through the center of the wave packet, are depicted in Fig. 5c, d. In comparison to the wave packet illustrated in Fig. 4, the wave packet depicted in Fig. 5 introduces an extra vortex in the $t - y$ domain, which induces an additional phase difference of π between the regions of $t < 0$ and $t > 0$ in the $t - x$ cross-section, as well as between the regions of $y > 0$ and $y < 0$ in the $x - y$ cross-section. It is worth noting that, to achieve more precise control over the orientation of OAM in 3D space, the l terms of the intersected vortices can take fractional values rather than being restricted to integer values.

Discussion

In summary, we report the generation of ST acoustic vortices with arbitrarily oriented OAM. We first extend ST acoustic vortices from 2D to 3D space, constructing ST wave packets carrying longitudinal and transverse OAM, respectively. The ST wave packet carrying tilted OAM can be obtained through the rotation of vortices in 3D space or the intersection of vortices carrying distinct types of OAM. The direction of OAM can be altered in the first method by adjusting the rotation angle or, in the second method, by modifying the OAM components in orthogonal directions. We experimentally generated ST wave packets using an acoustic phased array. By combining 2D spatial field scanning with 1D time-domain signal measurement, we achieved precise

characterization of 3D wave packets in the space-time domain. The direction of OAM serves as a new degree of freedom, expanding the capabilities for manipulating acoustic waves, with potential applications across various fields. Through the interaction between ST vortices and particles, it is possible to transfer OAM in arbitrary directions to particles, thereby achieving transient and arbitrary-directional particle manipulation. Shaping waves in the spatiotemporal domain with increasingly complex structures offers a promising avenue for research in both fundamental physics and applied sciences. Our work provides a platform for studying 3D acoustic wave fields with novel space-time structures, which will aid in the discovery and study of more exotic acoustic wave physics^{56–62}.

Methods

Generation of spatiotemporal (ST) vortices using the acoustic phased array

Using Fourier integration, a ST wave packet can be represented as a superposition of a series of plane wave modes:

$$p(x, y, z, t) = \iiint P(k_x, k_y, k_z) e^{ik_x x + ik_y y + ik_z z - i\omega(k)t} dk_x dk_y dk_z. \quad (8)$$

The spatial frequency spectrum can be obtained by performing a Fourier transform on the acoustic pressure field at $t = 0$, expressed

as follows:

$$P(k_x, k_y, k_z) = \int \int \int p(x, y, z, t = 0) e^{-ik \cdot r} dx dy dz. \quad (9)$$

By setting the width of the wave packet to $\frac{14}{k_0}$, the non-zero plane wave modes in the spatial frequency spectrum of ST wave packets mainly distribute within the intervals $[-0.3k_0, 0.3k_0]$ for k_x , $[-0.3k_0, 0.3k_0]$ for k_y , and $[k_0 - 0.3k_0, k_0 + 0.3k_0]$ for k_z . To generate ST wave packets using an acoustic phased array, we sample points in the spatial frequency spectrum. The wave vectors k_x , k_y , and k_z are sampled at equal intervals within the ranges of $[-0.3k_0, 0.3k_0]$, $[-0.3k_0, 0.3k_0]$, and $[k_0 - 0.3k_0, k_0 + 0.3k_0]$, with each interval containing 14 values. In this manner, we acquire 2744 plane wave modes represented by (k_x, k_y, k_z) . We drive the speaker array with the appropriately phased and amplitude-adjusted signals to generate acoustic plane wave modes steered in the desired directions. By superimposing these 2744 plane wave modes, the ST wave packet can be constructed.

Experimental setup

The experimental setup and measurement process are illustrated in Fig. 1c, e. We conduct experiments in an anechoic chamber covered with sound-absorbing materials on all sides to avoid unwanted reflections that could impact the experimental measurements. The 121 1.5-inch speakers are arranged in an 11×11 2D square grid with a spacing of 5.5 cm between each row and column [see Supplementary Fig. S1 for details]. The phased array is driven by four 32-channel sound cards (PreSonus Quantum 4848), all synchronized and controlled by a computer. Each speaker corresponds to a single channel on the sound card, allowing for individual control of each speaker's amplitude and phase. To improve measurement efficiency, we use the microphone array to capture the acoustic pressure field. The microphone array consists of 8 microphones (Knowles SPM0687LR5H-1), with a spacing of 9 cm between each microphone [see Supplementary Fig. S2 for details]. The microphone array is fixed on a 2D translation stage to measure the acoustic pressure field on the scan plane. The scan plane is parallel to the phased array and is positioned 20 cm away from it, with dimensions of approximately 70 cm by 70 cm. The translation stage moves in both the x and y directions with a step size of 1.5 cm. At each step, the phased array emits the same spatiotemporal wave packet, and the microphone array measures the time-domain acoustic pressure signals. Ultimately, the measurement points form a two-dimensional square grid with a spacing of 1.5 cm, covering the entire scan plane. The time-domain acoustic pressure signals are collected by the NI data acquisition module (NI 9234) at a sampling rate of 51.2 kHz. A trigger signal is generated simultaneously with the wave packet signal by the sound card and transmitted to the data acquisition module to initiate data collection, ensuring that each captured time-domain acoustic pressure signal is located within the same time interval. After the measurement is completed, the acoustic pressure field $p(x, y, t)$ can be obtained.

Data availability

All the data supporting the findings of this study are present in the paper and the supplementary information. Source data can be accessed on Zenodo at <https://doi.org/10.5281/zenodo.14906551>.

Code availability

The code in this paper is available from the corresponding author upon request.

References

- Allen, L., Beijersbergen, M. W., Spreeuw, R. J. C. & Woerdman, J. P. Orbital angular momentum of light and the transformation of Laguerre-Gaussian laser modes. *Phys. Rev. A* **45**, 8185–8189 (1992).
- Curtis, J. E. & Grier, D. G. Structure of Optical Vortices. *Phys. Rev. Lett.* **90**, 133901 (2003).
- Molina-Terriza, G., Torres, J. P. & Torner, L. Twisted photons. *Nat. Phys.* **3**, 305–310 (2007).
- Yao, A. M. & Padgett, M. J. Orbital angular momentum: origins, behavior and applications. *Adv. Opt. Photonics* **3**, 161 (2011).
- Shen, Y. et al. Optical vortices 30 years on: OAM manipulation from topological charge to multiple singularities. *Light Sci. Appl.* **8**, 90 (2019).
- Hefner, B. T. & Marston, P. L. An acoustical helicoidal wave transducer with applications for the alignment of ultrasonic and underwater systems. *J. Acoust. Soc. Am.* **106**, 3313–3316 (1999).
- Thomas, J.-L. & Marchiano, R. Pseudo Angular Momentum and Topological Charge Conservation for Nonlinear Acoustical Vortices. *Phys. Rev. Lett.* **91**, 244302 (2003).
- Gspan, S., Meyer, A., Bernet, S. & Ritsch-Marte, M. Optoacoustic generation of a helicoidal ultrasonic beam. *J. Acoust. Soc. Am.* **115**, 1142–1146 (2004).
- Marchiano, R. & Thomas, J.-L. Synthesis and analysis of linear and nonlinear acoustical vortices. *Phys. Rev. E* **71**, 066616 (2005).
- Jiang, X., Li, Y., Liang, B., Cheng, J. & Zhang, L. Convert Acoustic Resonances to Orbital Angular Momentum. *Phys. Rev. Lett.* **117**, 034301 (2016).
- Jiang, X. et al. Broadband and stable acoustic vortex emitter with multi-arm coiling slits. *Appl. Phys. Lett.* **108**, 203501 (2016).
- Zou, Z., Lirette, R. & Zhang, L. Orbital Angular Momentum Reversal and Asymmetry in Acoustic Vortex Beam Reflection. *Phys. Rev. Lett.* **125**, 074301 (2020).
- Uchida, M. & Tonomura, A. Generation of electron beams carrying orbital angular momentum. *Nature* **464**, 737–739 (2010).
- Clark, C. W. et al. Controlling neutron orbital angular momentum. *Nature* **525**, 504–506 (2015).
- Wang, J. et al. Terabit free-space data transmission employing orbital angular momentum multiplexing. *Nat. Photonics* **6**, 488–496 (2012).
- Shi, C., Dubois, M., Wang, Y. & Zhang, X. High-speed acoustic communication by multiplexing orbital angular momentum. *Proc. Natl. Acad. Sci.* **114**, 7250–7253 (2017).
- Wu, K. et al. Metamaterial-based real-time communication with high information density by multipath twisting of acoustic wave. *Nat. Commun.* **13**, 5171 (2022).
- Willig, K. I., Rizzoli, S. O., Westphal, V., Jahn, R. & Hell, S. W. STED microscopy reveals that synaptotagmin remains clustered after synaptic vesicle exocytosis. *Nature* **440**, 935–939 (2006).
- Invalone, G. et al. Free-Space Quantum Key Distribution by Rotation-Invariant Twisted Photons. *Phys. Rev. Lett.* **113**, 060503 (2014).
- He, H., Friese, M. E. J., Heckenberg, N. R. & Rubinsztein-Dunlop, H. Direct Observation of Transfer of Angular Momentum to Absorptive Particles from a Laser Beam with a Phase Singularity. *Phys. Rev. Lett.* **75**, 826–829 (1995).
- Padgett, M. & Bowman, R. Tweezers with a twist. *Nat. Photonics* **5**, 343–348 (2011).
- Hong, Z., Zhang, J. & Drinkwater, B. W. Observation of Orbital Angular Momentum Transfer from Bessel-Shaped Acoustic Vortices to Diphasic Liquid-Microparticle Mixtures. *Phys. Rev. Lett.* **114**, 214301 (2015).
- Marzo, A., Caleap, M. & Drinkwater, B. W. Acoustic Virtual Vortices with Tunable Orbital Angular Momentum for Trapping of Mie Particles. *Phys. Rev. Lett.* **120**, 044301 (2018).
- Bliokh, K. Y. & Nori, F. Spatiotemporal vortex beams and angular momentum. *Phys. Rev. A* **86**, 033824 (2012).
- Jhajj, N. et al. Spatiotemporal Optical Vortices. *Phys. Rev. X* **6**, 031037 (2016).
- Hancock, S. W., Zahedpour, S., Goffin, A. & Milchberg, H. M. Free-space propagation of spatiotemporal optical vortices. *Optica* **6**, 1547 (2019).

27. Chong, A., Wan, C., Chen, J. & Zhan, Q. Generation of spatio-temporal optical vortices with controllable transverse orbital angular momentum. *Nat. Photonics* **14**, 350–354 (2020).
28. Bliokh, K. Y. Spatiotemporal Vortex Pulses: Angular Momenta and Spin-Orbit Interaction. *Phys. Rev. Lett.* **126**, 243601 (2021).
29. Hancock, S. W., Zahedpour, S. & Milchberg, H. M. Mode Structure and Orbital Angular Momentum of Spatiotemporal Optical Vortex Pulses. *Phys. Rev. Lett.* **127**, 193901 (2021).
30. Huang, S., Wang, P., Shen, X., Liu, J. & Li, R. Diffraction properties of light with transverse orbital angular momentum. *Optica* **9**, 469 (2022).
31. Chen, W. et al. Time diffraction-free transverse orbital angular momentum beams. *Nat. Commun.* **13**, 4021 (2022).
32. Porras, M. A. Propagation of higher-order spatiotemporal vortices. *Opt. Lett.* **48**, 367 (2023).
33. Hancock, S. W., Zahedpour, S., Goffin, A. & Milchberg, H. M. Spatiotemporal Torquing of Light. *Phys. Rev. X* **14**, 011031 (2024).
34. Che, Z. et al. Generation of Spatiotemporal Vortex Pulses by Resonant Diffractive Grating. *Phys. Rev. Lett.* **132**, 044001 (2024).
35. Mazanov, M., Sugic, D., Alonso, M. A., Nori, F. & Bliokh, K. Y. Transverse shifts and time delays of spatiotemporal vortex pulses reflected and refracted at a planar interface. *Nanophotonics* **11**, 737–744 (2022).
36. Hancock, S. W., Zahedpour, S. & Milchberg, H. M. Second-harmonic generation of spatiotemporal optical vortices and conservation of orbital angular momentum. *Optica* **8**, 594 (2021).
37. Gui, G., Brooks, N. J., Kapteyn, H. C., Murnane, M. M. & Liao, C.-T. Second-harmonic generation and the conservation of spatio-temporal orbital angular momentum of light. *Nat. Photonics* **15**, 608–613 (2021).
38. Fang, Y., Lu, S. & Liu, Y. Controlling Photon Transverse Orbital Angular Momentum in High Harmonic Generation. *Phys. Rev. Lett.* **127**, 273901 (2021).
39. Chen, J., Wan, C. & Zhan, Q. Engineering photonic angular momentum with structured light: a review. *Adv. Photonics* **3**, 064001 (2021).
40. Wang, H., Guo, C., Jin, W., Song, A. Y. & Fan, S. Engineering arbitrarily oriented spatiotemporal optical vortices using transmission nodal lines. *Optica* **8**, 966 (2021).
41. Huang, J., Zhang, J., Zhu, T. & Ruan, Z. Spatiotemporal Differentiators Generating Optical Vortices with Transverse Orbital Angular Momentum and Detecting Sharp Change of Pulse Envelope. *Laser Photonics Rev.* **16**, 2100357 (2022).
42. Huang, J., Zhang, H., Wu, B., Zhu, T. & Ruan, Z. Topologically protected generation of spatiotemporal optical vortices with nonlocal spatial mirror symmetry breaking metasurface. *Phys. Rev. B* **108**, 104106 (2023).
43. Liu, W. et al. Exploiting Topological Darkness in Photonic Crystal Slabs for Spatiotemporal Vortex Generation. *Nano Lett.* **24**, 943–949 (2024).
44. Huo, P. et al. Observation of spatiotemporal optical vortices enabled by symmetry-breaking slanted nanograting. *Nat. Commun.* **15**, 3055 (2024).
45. Wan, C., Chen, J., Chong, A. & Zhan, Q. Photonic orbital angular momentum with controllable orientation. *Natl. Sci. Rev.* **9**, nwab149 (2022).
46. Zang, Y., Mirando, A. & Chong, A. Spatiotemporal optical vortices with arbitrary orbital angular momentum orientation by astigmatic mode converters. *Nanophotonics* **11**, 745–752 (2022).
47. Porras, M. A. & Jolly, S. W. Control of vortex orientation of ultrashort optical pulses using a spatial chirp. *Opt. Lett.* **48**, 6448 (2023).
48. Demore, C. E. M. et al. Mechanical Evidence of the Orbital Angular Momentum to Energy Ratio of Vortex Beams. *Phys. Rev. Lett.* **108**, 194301 (2012).
49. Baresch, D., Thomas, J.-L. & Marchiano, R. Observation of a Single-Beam Gradient Force Acoustical Trap for Elastic Particles: Acoustical Tweezers. *Phys. Rev. Lett.* **116**, 024301 (2016).
50. Volke-Sepúlveda, K., Santillán, A. O. & Boulosa, R. R. Transfer of Angular Momentum to Matter from Acoustical Vortices in Free Space. *Phys. Rev. Lett.* **100**, 024302 (2008).
51. Marzo, A. et al. Holographic acoustic elements for manipulation of levitated objects. *Nat. Commun.* **6**, 8661 (2015).
52. Fu, Y. et al. Asymmetric Generation of Acoustic Vortex Using Dual-Layer Metasurfaces. *Phys. Rev. Lett.* **128**, 104501 (2022).
53. Ge, H. et al. Spatiotemporal Acoustic Vortex Beams with Transverse Orbital Angular Momentum. *Phys. Rev. Lett.* **131**, 014001 (2023).
54. Zhang, H. et al. Topologically crafted spatiotemporal vortices in acoustics. *Nat. Commun.* **14**, 6238 (2023).
55. Bliokh, K. Y. Orbital angular momentum of optical, acoustic, and quantum-mechanical spatiotemporal vortex pulses. *Phys. Rev. A* **107**, L031501 (2023).
56. Wang, J. et al. Spatiotemporal Single-Photon Airy Bullets. *Phys. Rev. Lett.* **132**, 143601 (2024).
57. Chen, W. et al. Observation of Chiral Symmetry Breaking in Toroidal Vortices of Light. *Phys. Rev. Lett.* **132**, 153801 (2024).
58. Yessenov, M., Hall, L. A., Schepler, K. L. & Abouraddy, A. F. Space-time wave packets. *Adv. Opt. Photonics* **14**, 455 (2022).
59. Shen, Y. et al. Roadmap on spatiotemporal light fields. *J. Opt.* **25**, 093001 (2023).
60. Huang, S. et al. Spatiotemporal vortex strings. *Sci. Adv.* **10**, eadn6206 (2024).
61. Liu, X. et al. Spatiotemporal optical vortices with controllable radial and azimuthal quantum numbers. *Nat. Commun.* **15**, 5435 (2024).
62. Cao, Q., Zhang, N., Chong, A. & Zhan, Q. Spatiotemporal hologram. *Nat. Commun.* **15**, 7821 (2024).

Acknowledgements

The work is jointly supported by the National Key R&D Program of China [Grants No. 2023YFA1406904 (M.-H.L.) and 2021YFB3801801 (Y.-F.C.)], the Key R&D Program of Jiangsu Province [Grants No. BK20232048 (H.G.) and BK20232015 (H.G.)], and the National Natural Science Foundation of China [Grants No. 52250363 (M.-H.L.) and 52203358 (H.G.)].

Author contributions

H.G., M.-H.L., and Y.-F.C. conceived the original idea and supervised this project. S.L. performed the theoretical calculations. S.L., H.G., X.-Y.X. and Y.S. carried out the experiments. S.L., H.G. and M.-H.L. analyzed the data. S.L. and H.G. wrote the manuscript with the assist of X.-P.L. All authors contributed to scientific discussions of the manuscript.

Competing interests

The authors declare no competing interests.

Additional information

Supplementary information The online version contains supplementary material available at <https://doi.org/10.1038/s41467-025-58154-1>.

Correspondence and requests for materials should be addressed to Hao Ge, Ming-Hui Lu or Yan-Feng Chen.

Peer review information *Nature Communications* thanks Alexander Volgar and the other anonymous reviewer(s) for their contribution to the peer review of this work. A peer review file is available.

Reprints and permissions information is available at <http://www.nature.com/reprints>

Publisher's note Springer Nature remains neutral with regard to jurisdictional claims in published maps and institutional affiliations.

Open Access This article is licensed under a Creative Commons Attribution-NonCommercial-NoDerivatives 4.0 International License, which permits any non-commercial use, sharing, distribution and reproduction in any medium or format, as long as you give appropriate credit to the original author(s) and the source, provide a link to the Creative Commons licence, and indicate if you modified the licensed material. You do not have permission under this licence to share adapted material derived from this article or parts of it. The images or other third party material in this article are included in the article's Creative Commons licence, unless indicated otherwise in a credit line to the material. If material is not included in the article's Creative Commons licence and your intended use is not permitted by statutory regulation or exceeds the permitted use, you will need to obtain permission directly from the copyright holder. To view a copy of this licence, visit <http://creativecommons.org/licenses/by-nc-nd/4.0/>.

© The Author(s) 2025